Depletion of tumor-derived CXCL5 improves T cell infiltration and anti-PD-1 therapy response in an obese model of pancreatic cancer

Richard McKinnon Walsh [ORCID],[1] Joseph Ambrose,[1] Jarrid L Jack,[1] Austin E Eades [ORCID],[1] Bailey A Bye,[1] Mariana Tannus Ruckert [ORCID],[1] Fanuel Messaggio,[2] Appolinaire A Olou,[1] Prabhakar Chalise [ORCID],[3,4] Dong Pei,[3,4] Michael N VanSaun [ORCID][1,2]

[1]Cancer Biology, KUMC, Kansas City, Kansas, USA
[2]Department of Surgery, University of Miami Miller School of Medicine, Miami, Florida, USA
[3]Biostatistics and Data Science, University of Kansas Medical Center, Kansas City, Kansas, USA
[4]The University of Kansas Cancer Center, Kansas City, Kansas, USA

Correspondence to
Dr Michael N VanSaun;
mvansaun@kumc.edu

ABSTRACT

Background CXCR1/2 inhibitors are being implemented with immunotherapies in PDAC clinical trials. CXC-ligands are a family of cytokines responsible for stimulating these receptors; while typically secreted by activated immune cells, fibroblasts, and even adipocytes, they are also secreted by immune-evasive cancer cells. CXC-ligand release is known to occur in response to inflammatory stimuli. Adipose tissue is an endocrine organ and a source of inflammatory signaling peptides. Importantly, adipose-derived cytokines and chemokines are implicated as potential drivers of tumor cell immune evasion; cumulatively, these findings suggest that targeting CXC-ligands may be beneficial in the context of obesity.
Methods RNA-sequencing of human PDAC cell lines was used to assess influences of adipose conditioned media on the cancer cell transcriptome. The adipose-induced secretome of PDAC cells was validated with ELISA for induction of CXCL5 secretion. Human tissue data from CPTAC was used to correlate IL-1β and TNF expression with both CXCL5 mRNA and protein levels. CRISPR-Cas9 was used to knockout CXCL5 from a murine PDAC KPC cell line to assess orthotopic tumor studies in syngeneic, diet-induced obese mice. Flow cytometry and immunohistochemistry were used to compare the immune profiles between tumors with or without CXCL5. Mice-bearing CXCL5 competent or deficient tumors were monitored for differential tumor size in response to anti-PD-1 immune checkpoint blockade therapy.
Results Human adipose tissue conditioned media stimulates CXCL5 secretion from PDAC cells via either IL-1β or TNF; neutralization of both is required to significantly block the release of CXCL5 from tumor cells. Ablation of CXCL5 from tumors promoted an enriched immune phenotype with an unanticipatedly increased number of exhausted CD8 T cells. Application of anti-PD-1 treatment to control tumors failed to alter tumor growth, yet treatment of CXCL5-deficient tumors showed response by significantly diminished tumor mass.
Conclusions In summary, our findings show that both TNF and IL-1β can stimulate CXCL5 release from PDAC cells in vitro, which correlates with expression in patient data. CXCL5 depletion *in vivo* alone is sufficient to promote T cell infiltration into tumors, increasing efficacy and

WHAT IS ALREADY KNOWN ON THIS TOPIC

⇒ Obesity is linked to a worsened patient outcome and associated with an immune evasive tumor profile in PDAC. CXCR1/2 inhibitors have begun to be implemented in combination with immune checkpoint blockade therapies clinically; these were driven by studies targeting tumor-intrinsic CXCR2 signaling and CXCL1 expression to promote T cell infiltration.

WHAT THIS STUDY ADDS

⇒ Using *in vitro/ex vivo* cell and tissue culture-based assays, we have identified that adipose-derived IL-1β and TNF can promote tumor secretion of CXCL5. CXCL5 depletion enhanced CD8 T cell tumor infiltration as expected. Contrary to expected results, CXCL5 loss surprisingly led to a more immune-suppressive MDSC profile within the tumors; this correlated with enhanced CD8 T PD1 positivity.

HOW THIS STUDY MIGHT AFFECT RESEARCH, PRACTICE OR POLICY

⇒ This study highlights a novel CXCL5-driven T cell regulatory mechanism and assesses the efficacy of targeting a single CXCR1/2 ligand to overcome tumor immune evasion.

requiring checkpoint blockade inhibition to alleviate tumor burden.

BACKGROUND

Pancreatic cancer is projected to become the second leading cause of cancer-associated death in the United States by 2030, despite being projected to be eleventh in incidence.[1] High body mass index (BMI) correlates with earlier incidence and poorer outcome in retrospective studies of Pancreatic Ductal Adenocarcinoma (PDAC)[2][3]; obesity is a risk factor enhancing tumor progression of PDAC, among other cancers.[4–8] Obesity encompasses the induction of inflammation

in adipose tissue and is thus termed "reactive adipose" that results in a consequential altered secretion of adipose tissue-derived cytokines ("adipokines") derived from adipocytes or adipocyte-associated immune cells.[9 10] The direct influence of adipokines on cancer-cell-intrinsic, pro-tumorigenic properties has been well documented in a variety of contexts.[4 11 12] Secondary effects of adipokines that alter the tumor's relationship with other cells in the tumor microenvironment (TME) and systemic effects are only more recently being investigated.[13] Of those, adipose-derived IL-1β has been shown to be responsible for prevention of T-cell infiltration in obese PDAC mouse models: blockade of IL-1β rescues T cell recruitment while limiting monocyte (CD11b/Ly6G+) presence.[6] Adipose that is rich in secretory monocytes is not the only source of common adipokines; within the TME itself, intratumoral myeloid cells have been shown to source IL-1β and drive immune-evasive signaling preventing T cell infiltration, supplemental to TNF contribution from myeloid and fibroblast populations. Because T cell infiltration into PDAC tumors is often poor, checkpoint blockade inhibitors (CBIs) have been ineffective in preclinical models without additional perturbation of the tumor or microenvironment.[14–17] Therefore, determining mechanisms of enhancing T cell recruitment to the TME is recognized as an important strategy in PDAC research.

Successful implementation of immunotherapeutic sensitivity has focused toward modifying myeloid populations; predominantly through the blockade of CXCR1/2 and its ligands, which are often over-expressed in PDAC.[18–24] Preclinical studies in PDAC have shown impressive results in targeting CXCR1/2 ligands such as CXCL1, CXCL2, or CXCL8.[18 22–26] Specifically, CXCL1, 2, 5, and 8 are elevated in PDAC tumors. While CXCL2 has been reported to be derived from the stroma,[27] CXCL1 is sourced by immune evasive cancer cells, as well as cancer-associated fibroblasts (CAFs) and is reported to prevent tumorous T cell infiltration in PDAC via myeloid-derived suppressor cell (MDSC) recruitment through myeloid specific CXCR2 enrichment.[18 26 28 29] Recently, CXCL8 has been shown to be expressed by both granulocytes and in specific E-cadherin positive pancreatic cancer cells in human tumors: higher expression of CXCL8 within the tumor was further associated with worsened patient outcome.[30] Other studies have shown the importance of CXCR2 in facilitating PDAC growth/metastasis, and CXCR2 targeting genetically or pharmacologically increases T cell infiltration.[23 31 32] This has been attributed to CXCR2 expression on both the myeloid immune compartment and intrinsic cancer cell expression of CXCR2 and ligands CXCL1, CXCL2, and CXCL8.[23 29–34]

Current clinical trials are testing the efficacy of CXCR1/2 inhibition combined with CBIs across multiple cancer types.[24] CXCL5 is another CXCR1/2 ligand that drives neutrophil recruitment and activation to sites of inflammation and is associated with reduced survival probability in multiple cancers, including PDAC.[19 35 36] CXCL5 has been shown to promote T cell inhibitory neutrophil recruitment in lung cancer models and is correlated with immune-inhibitory gene expression patterns in PDAC.[36 37]

In this study, we show that cancer cell secretion of CXCL5 can be directly induced by IL-1β or TNF, which are abundant in adipose tissue. We used a combination of InVivoMAb anti-mouse PD-1 (CD279) CBI combined with a depletion of CXCL5 by Crispr-Cas9-mediated knockout to interrogate the contribution of tumor-derived CXCL5 to susceptibility for immunotherapy in an obese setting.

METHODS

Detailed methods are described in online supplemental material, here in brief:

Cell culture

Cell lines MiaPaCa2, HPNE-G12D, Panc1, HEK-293T, cell lines were acquired and used within 15 passages from purchase (ATCC). K8484 cell line was a gift from Dr. Dave Tuveson.[38] Cells were grown in high-glucose+pyruvate DMEM (Gibco#11 995 073), supplemented with Antibiotic-Antimycotic (Anti-Anti) (Gibco#15 240 062) and 5%–10% Fetal Bovine Serum (FBS) (Biowest#S1620) ("complete") at 37°C in 5% CO_2, and routinely monitored for mycoplasma.

Patient-derived human adipose tissue conditioned media collection

Patient samples were provided by the KUMC Biospecimen Repository Core Facility (IRB HSC #5929). Peripancreatic-adipose tissue was collected during tumor resection, kept at room temperature (RT) in PBS until processing. Gross peripancreatic adipose was washed 3× in RT-PBS+Anti-Anti+10 µg/mL Ciprofloxacin (Santa Cruz#29 064), then cut into small sections. Adipose was incubated 30–60 min in 5–10 mL of serum-free (SF) DMEM+anti-anti+ciprofloxacin to clear factors released due to manipulation.[39] A 1 mL SF-DMEM+anti-anti+ciprofloxacin was added per 125 mg of tissue in a tissue culture plate and incubated for 24 hours at 37°C+5%CO_2. Human adipose tissue conditioned media (hAT-CM) was collected, spun at 300×g for 5 min, then 5000×g for 5 min. The media was sterile filtered (0.22 µM filter (Rephile#RJP3222NH)), aliquoted, and stored at −80°C. hAT-CM was used at a ratio of 1:3-1:5 hAT-CM:SF-DMEM. Staging, sex, BMI, neoadjuvant treatment status, adjuvant treatment, and associated experiments for each hAT-CM sample are reported in online supplemental methods and online supplemental table 1.

Proliferation assays

Proliferation was measured by EdU incorporation as previously described.[40] Briefly, cells were treated for 24 hours with hAT-CM (1:3 hAT-CM:SF-DMEM) or media. EdU was added for 6 hours. Cells were trypsinized and fixed overnight in 1.5% Buffered Formalin at 4°C. Cells were permeabilized and underwent Click-It reaction using $CuSO_4$ (Alfa-Aesar#14178) and 647 Azide-Dye

(Invitrogen#A10277), counter-stained with propidium iodide (ThermoFisher#P3566) and measured for fluorescence by flow cytometry.

RNA-seq sample preparation
Cells were distributed at 1E6/well in six-well plates. The next day, cells were washed then treated with SF-DMEM+anti anti, or hAT-CM from individual patients (not pooled) diluted 1:3 using SF-DMEM+anti anti as diluent for 24 hours, washed, then lysed in QIA-zol (Qiagen#51-13-02). RNA was extracted using the Direct-zol RNA Miniprep Kit (Zymo Research#R2052) following the manufacturer's protocol.

Library prep was completed following Tecan Universal Plus mRNA library Prep (Stranded mRNA Library), then sequenced on a NovaSeq S1-200 cycle (100PE) flow cell using XP 2-lane chemistry for independent lane loading. Groupings of samples were MiaPaCa2, Panc1, and HPNE-G12D. Batch effects were corrected using the ComBat-seq method[41] prior to statistical analysis.

RNAseq quality control, differential expression
For each sample, quality control was conducted by using FastQC (http://www.bioinformatics.babraham.ac.uk/projects/fastqc). Samples that passed quality control were aligned to human genome hg38 with RSEM[42] and bowtie2.[43] Counts were used for downstream analysis. Prior to differential expression (DE) analysis, non-expressed genes (low: zero counts) were filtered out to remove biologically uninteresting genes and attenuate the burden of multiple testing. DE analyses among groups were performed using a generalized linear model based on negative binomial distribution in *edgeR*. Pairwise comparisons were performed by specifying appropriate contrast statements in the modeling framework. Multiple-testing adjustments were made using Benjamini-Hochberg's False-Discovery-Rate method. Volcano plots were prepared from each comparison. Pathway analysis was performed using Qiagen Ingenuity Pathway Analysis (IPA).

ELISAs
Initial CXCL5 ELISA samples were collected after cells were washed, then treated with 1:3 diluted hAT-CM for 24 hours.[44] Blocking assay: Panc1 cells were plated at 60k/well on a 48-well plate. The next day, cells were preincubated for 1 hour in 2.5% FBS media at 37°C, then washed prior to hAT-CM or treatment. Conditioned media/recombinant protein treatment of cells for CXCL5 release was performed with 1:4 dilution of pooled hAT-CM:SF-DMEM+1.5% BSA (Rockland#BSA-30) and collected at 36 hours.[44] Media was centrifuged at 1000xg to remove cells/debris, then measured for CXCL5 by ELISA (R&D Systems#DY254,#DY008B) according to the manufacturer's protocol. Recombinant human TNF (PeproTech#300–01A) and IL-1β (PeproTech#200-01B) were applied at 1µg/mL. Blocking antibodies against TNF (CST#7321S) and IL-1β (abcam#ab9722) or IgG (Santa Cruz#sc-2027) were applied at 1µg/mL. TNF (R&D Systems#DY210-05) and IL-1β (R&D Systems#DY201-05) ELISAs of hAT-CM were performed according to the manufacturer's protocols.

Lentivirus production
HEK-293T (ATCC) cells were treated according to the Lipofectamine-3000 protocol with Opti-MEM (Gibco#31985070) and Lipofectamine (Invitrogen#L3000001)+plasmid DNA (Addgene: Lenti-Cas9#52962; Lenti-envelope#8454; Lenti-backbone#8455) to produce virus then concentrated with Lenti-X concentrator (TakaraBio#631231).

CRISPR/Cas9 knockout of CXCL5
TransOMIC technologies CCMS1001 kit was used for generation knockout cells. Two separate guide RNAs (TransOMIC technologies#TEVM-1096303 ("3"), TEVM-1163445 ("45")) were selected and used to generate four CXCL5-knockout clones.

Sequences: NTC (GGAGCGCACCATCTTCTTCA), "3" (ATGGCGAGATGGAACCGCTG), "5" (GTTCCATCTCGCCATTCATG).

K8484[38] cells were transfected with a lenti-viral, blasticidin-resistant Cas9 cassette (Addgene#52962) and selected in 10µg/mL Blasticidin. Selected cells were transfected with puromycin-resistant CXCL5 or NTC gRNA. Single cell colonies were selected with 10µg/mL Puromycin (Gibco#A1113803). Two clones from each CXCL5 guide were used.

qPCR and quantification
qPCR was performed according to the APExBIO HotStart 3-step protocol (APExBIO#K1070) in a ViiA-7 Real-Time PCR System (ThermoFisher). Quantification was performed by Livak method[45] (GAPDH=reference). Primers: Qiagen #QT01658146 (CXCL5), #QT01658692 (GAPDH).

Animal studies
In total, 42 mice were used in this study (online supplemental table 2).

Diet-induced obesity
Jax/BL6 (Jax#000664) mice at 6–8 weeks old were put on a Western-style High-Fat Diet (HFD) (Teklad-Envigo InotivCo#TD.88137), Adjusted Calories Diet (42% kcal fat, 34% sucrose weight) for a minimum of 3 months and maintained on HFD through experiment endpoint.

Orthotopic pancreatic tumor model
1-2E6 cells were pelleted at 1k×*g* for 3min and kept on ice until resuspension. Mice were anesthetized using 3%–5% Isoflurane (Patterson#14043070406), preoperatively administered 50µL of Buprenorphine for pain relief. The surgery site was cleared of fur and sterilized with Povidone-Iodine (Dynarex#1108) and Isopropanol (Medi-First#22133). Cells were resuspended in 100µL Geltrex (Gibco#A1413202). 50µL cell/Geltrex

solution was injected into the pancreas using a 27 Gx½ inch needle (BD#305 109). The peritoneum was sutured with 5-0 DemeCRYL (DemeTECH#G175016F13M); skin stapled with an AutoClip (Fine Science Tools#12020-09, 12022-09). The wound site was treated with triple antibiotic ointment (Akorn).

Tumor dissociation for immune cell isolation
Pancreas/tumors were removed from mice, sections were fixed in 10% buffered formalin overnight or frozen at −80°C; the remainder was used for immune isolation. Tumors were minced via razor blade (FisherSci#12-640), washed in 10 mL of SF-RPMI-1640 (Gibco#A1049101)+1 mg/mL Soybean Trypsin Inhibitor (Sigma-Aldrich#T6522-1G). Minced tumors were centrifuged 350xg for 10 min, resuspended in 5 mL of Digest Solution (online supplemental methods) and shaken 150–200 rpm 25–35 min at 37°C. Digestion was halted with complete media, filtered through 100 µm–40 µm strainers (Research Products International Corp#162427100, 162425100). Dissociated tumors were spun at 350x*g* for 20 min and resuspended in 1 mL autoMACS Running Buffer+120 U/mL DNaseI.

Spleen dissociation for immune cell isolation
Spleens were dissociated using a gentleMACS Dissociator (Miltenyi#130-093-235) in autoMACS Running Buffer in gentleMACS C-Tubes (Miltenyi#130-093-237) (m_Spleen_01 protocol). Dissociated spleens were washed in autoMACS buffer and spun at 350×*g* for 10 min. Cells were resuspended in 10 mL RBC Lysis Buffer (Biolegend#420301), vortexed, and incubated at RT for 10 min. The cells were centrifuged 350×*g* for 10 min and resuspended in 10 mL autoMACS buffer+DNaseI. The cells were filtered through 100 µm then 40 µm strainers, centrifuged 350×*g* for 10 min, then resuspended in autoMACS buffer+DNaseI.

Cell staining for flow cytometry
Antibody panels are outlined in online supplemental figure 4B. Isolated cells in autoMACS buffer were transferred to microfuge tubes and centrifuged 400x*g* for 10 min, then resuspended in 1 mL of 10 µL/mL TruStain FcX PLUS (Biolegend#156604) blocking at RT for 20 min rocking. Blocked cells were spun 400xg, resuspended in autoMacs+DNase, and distributed to tubes for each immune panel and stained 20 min at RT in a darkbox. Cells were washed and fixed overnight at 4°C. The next day, cells were washed again and stored at 4°C until analyzed on a BD LSR-II four-laser (405, 488, 552, 637 nm) cytometer. Compensation controls were prepared using spleens or Ultracomp eBeads (Thermo#01-2222-42).

In vivo PD-1 administration
Anti-mouse PD-1 (BioXCell#BE0273, Clone#29F.1A12) or IgG (BioXCell#BE0089) was diluted in *InVivo*Pure pH 7.0 Dilution Buffer (BioXCell#IP0070) to 200 µg/100 µL treated with 100 µL (200 µg) per mouse[46] on day 10, day 13, day 16, day 19, and day 22 following tumor implantation

based on reported effective dosage by the manufacturer's reference.[47] The antibody was delivered by intraperitoneal injection via 28G½-inch syringe (BD#329461).

Immunofluorescent staining of paraffin-embedded tissues
Antibody info: Paraffin-embedded formalin-fixed tissue section slides were cleared/rehydrated with Histo-Clear (Electron Microscopy Sciences#64110), and ethanol series then permeabilized. Antigen retrieval was performed in citrate overnight at 60°C in a water bath, or microwaved at power level 4 for 12 min. Slides were blocked then incubated with primary antibody. Slides were washed and stored in TBS at 4°C until secondary antibody and Hoechst (Invitrogen#H3570) stained 1h at RT. Stained slides were washed then incubated in Sudan Black to quench background and imaged on an EVOS m5000 microscope.

Statistical analysis
Statistical tests were performed as indicated in figure legends using GraphPad Prism V.9.0: Distribution of CPTAC samples was assessed for Gaussian distribution in GraphPad Prism. Two sample T-tests were used to compare across two groups (Welch's or Mann-Whitney). Comparisons across multiple groups were carried out using one-way analysis of variance with Browne-Forsythe and Welch corrections. Replicates are denoted in figure legends. TCGA data were accessed, and Kaplan-Meier curve figures were generated using GEPIA, which provided statistical testing with figure generation of time to event outcome data (dataset).[48] CPTAC proteogenomic data were accessed via cProSite.cancer.gov and Proteomic Data Commons (dataset),[49 50] organized in Microsoft Excel, then visualized for presentation and assessed for statistical significance in GraphPad Prism V.9.0. Statistical tests were considered significant if the p value is less than 0.05.

RESULTS
Adipose conditioned media from PDAC patients promotes proliferation and CXCL5 secretion
To determine whether adipose factors directly influence pancreatic cancer cells, we employed conditioned-media transfer experiments. Adipose tissue was collected from PDAC patients during surgical resection and cultured in SF media (figure 1A). Human adipose tissue conditioned media (hAT-CM) was diluted and applied to human PDAC (MiaPaCa2, Panc1) or an immortalized ductal (HPNE-G12D) cell lines measuring proliferation by EdU incorporation (figure 1B). hAT-CM treatment was sufficient to stimulate proliferation of PDAC cell lines but failed to stimulate proliferation of HPNE-G12D cells above that of SF media.

We next took media from MiaPaCa2 cells treated with hAT-CM and screened a cytokine array to identify changes to the secretome of the PDAC cells in response to the hAT-CM stimulation (online supplemental figure
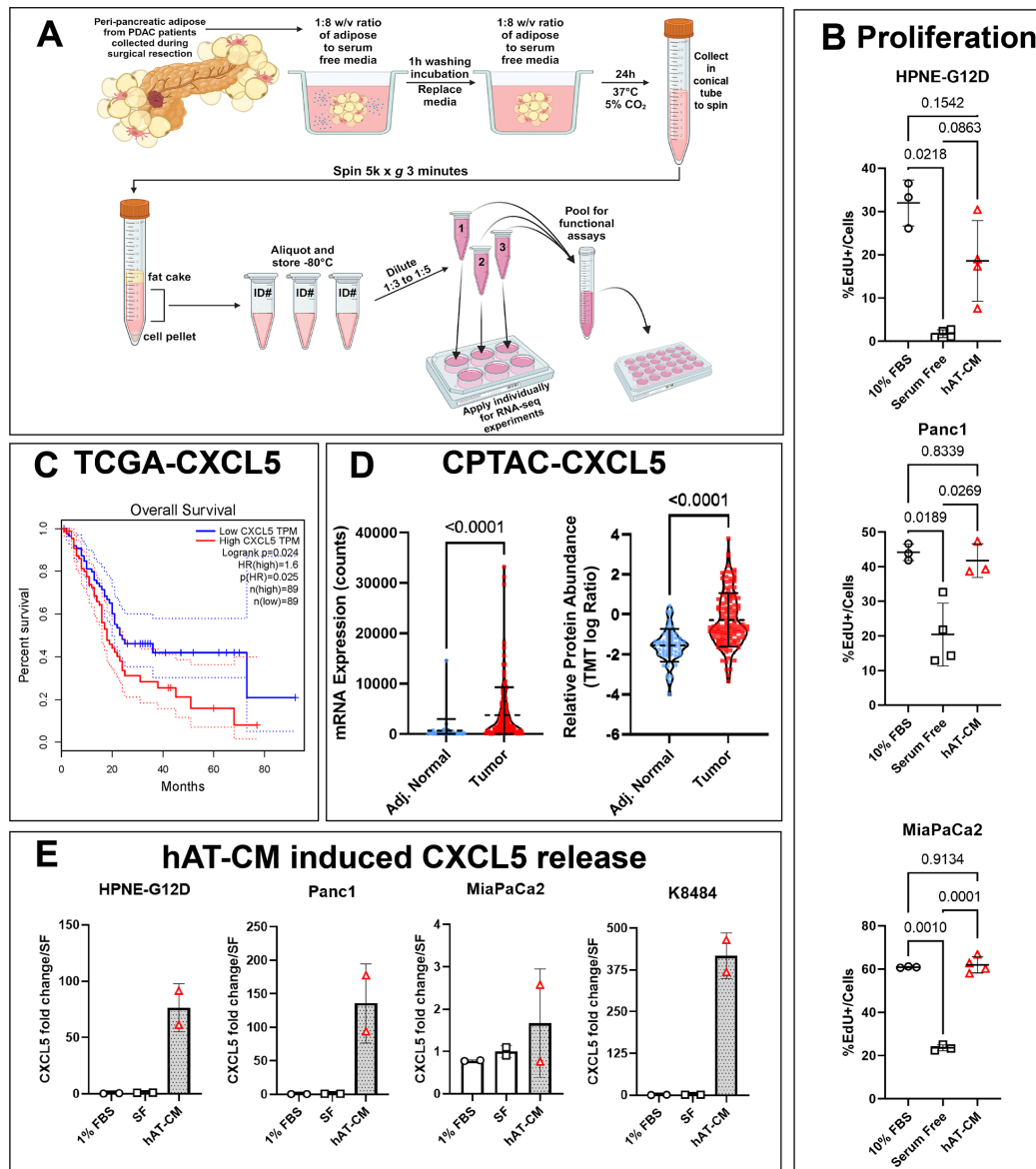
Figure 1 (A) Schematic (Created in BioRender Walsh, R (2024) https://BioRender.com/o20p233) illustrating human adipose tissue conditioned media (hAT-CM) collection, storage, and application. Human adipose tissue is incubated in serum-free media at a 1:8 w/v ratio for 1 hour as a wash, then incubated for 24 hours in fresh serum-free media to collect adipose-associated factors. Media is collected and spun to remove cells and debris, then aliquoted, frozen, and diluted for application in functional assays. (B) Proliferation measured by flow cytometry for EdU incorporation into cells in vitro in response to stimulus with pooled hAT-CM diluted 1:3 in Serum Free DMEM (red triangles), Serum Free DMEM (black open squares), or 10% fetal bovine serum (FBS) supplemented DMEM (black open circles). Immortalized pancreatic ductal HPNE-G12D cells and Pancreatic Ductal Adenocarcinoma (PDAC) tumor cell lines (Panc1 and MiaPaCa2) were treated with diluted hAT-CM, serum-free media, or complete media for 24 hours. Then, EdU was spiked and mixed into the media to reach a final concentration of 10 µM for 6 hours to measure incorporation and active proliferation by flow cytometry to show that hAT-CM can induce proliferation of cancer cells in vitro: PI was used as a counter stain following fixation and permeabilization to quantify the total number of cells, and double positive EdU+PI+ events were quantified as a percentage of total PI+events. (C) Kaplan-Meier plot for CXCL5 high or low patients was generated using GEPIA showing significant differences in overall survival between the upper and lower half expressing patients in the PAAD-TCGA dataset±CI, p=0.024, n=89 patients for each dataset compared. (D) mRNA (left) and relative protein abundance (right) of normal (blue) and tumor (red) tissue shows increased mRNA expression and protein abundance of CXCL5 in tumor compared with adjacent normal tissue (CPTAC-cProSite). mRNA expression: n=39 for normal, n=138 for tumor; protein abundance: n=65 for normal, n=135 for tumor. The dashed line across each sample represents mean expression or abundance. (E) 24-hour stimulation of cells with hAT-CM shows CXCL5 in the media of the stimulated cells measured by ELISA normalized to serum free (SF) values, or compared with treatment with 1% FBS containing media; n=2 wells per treatment. Statistical analyses were performed using Brown-Forsythe and Welch corrected one-Way ANOVA in GraphPad Prism for (B) (EdU proliferation). CPTAC data (D) failed normality testing (S1D-E), therefore, the Mann-Whitney test was applied to CPTAC data to compare normal and tumor mRNA and protein abundance. P values <0.05 were considered significant and displayed up to four decimals. Error bars represent SD. ANOVA, analysis of variance.

1A). CXCL5 was identified among differential targets compared with untreated cells and selected for further evaluation. TCGA data have been evaluated showing higher tumor CXCL5 expression is correlated to poor patient outcome.[19 36 48] While other CXCR1/2 ligands trend toward a correlative effect, they failed to meet statistical significance (figure 1C, online supplemental figure 1B) (dataset).[48] CXCL5 showed higher expression in tumor compared with normal tissue in CPTAC RNA data, and greater abundance in TMT-proteomic data procured using cProSite[49] across bulk comparison of tumor versus normal (figure 1D). Plotting of CXCL5 protein by stage was statistically insignificant (p=0.069) but showed a positive trend (online supplemental figure 1C). Together, these data show that CXCL5 is presented in PDAC in patients and in a tissue culture setting.

IL-1β and TNF signaling are implicated as pathway activators responsible for transcriptional changes in response to hAT-CM

RNA-seq was performed on cell lines following treatment with hAT-CM collected from eight individual PDAC patients versus culturing in SF conditions to assess tumor-intrinsic alterations and predict upstream drivers of the resulting transcriptional profiles ((dataset) Gene Expression Omnibus ncbi.nlm.nig.gov/geo 288 Accession Number: GSE274713). hAT-CM from each patient was treated in a separate well, and the eight collective biological replicates were compared against cells treated only in SF media. While sex and stage were unreported for two of the eight samples assessed, the experiment included four male and three female patients, with one stage IB, one stage IIB, and one stage III sample from each sex, and an additional stage IIB male sample. Additionally, all samples reported no neoadjuvant therapy, except for one sample that was labeled as unreported. BMI varied across both sexes and is reported in online supplemental table 1. Qiagen IPA was used to identify potential upstream regulators driving transcriptional changes in hAT-CM treated cells. IL-1β and TNF were identified as potential drivers of differential transcription between SF or hAT-CM treated cells consistent across the three cell lines (figure 2). Panc1 cells had the most robust response to hAT-CM, yet similarities were identified across all three cell lines (figure 2B): IL-1β and TNF demonstrated the strongest upstream-analysis scoring among the three groups (figure 2C). Additional hAT-CM was collected and assessed by ELISA for overweight/obese versus lean hAT-CM, which failed to show expected[51] differential IL-1β or TNF levels (online supplemental figure 2B), but did show large quantities being produced by the adipose tissue regardless of BMI, concurrent with the mixed BMI status of the RNAseq hAT-CM dataset (online supplemental table 1). Of note, TNF levels were endogenously expressed in response to hAT-CM treatment in MiaPaCa2 cells but were undetected in Panc1 and HPNE-G12D cells (online supplemental table 3). hAT-CM, therefore, may be contributing to differential subsequent autocrine effects among cell lines. We then assessed for sex-specific hAT-CM induced transcriptional pathways by comparing transcripts from cells treated with either hAT-CM derived from female or male patients. While there were significant differentially expressed genes (online supplemental figure 2F), those associated with chemokine/cytokine signaling pathway activation were inconsistent, absent, or conflicting across the cell lines (online supplemental table 4).

Whole tumor IL-1β and TNF are associated with enhanced CXCL5 expression in patient data, but only tumor-intrinsic TNF expression in cell lines

mRNA levels of TNF and IL-1β in patient CPTAC data show a weak but significant correlation with CXCL5 mRNA levels but show a slightly stronger correlation with CXCL5 protein data (figure 3A) (dataset).[48–50] TNF and IL-1β were not detected by proteomic quantification in these samples, thus not included. TNF displays stronger correlation with cell line data accessed from the DepMap portal across 50 PDAC cell lines tested, while tumor cell intrinsic IL-1β seems to have no correlation with PDAC CXCL5 expression (online supplemental figure 2D,E).

Blockade of adipose-derived IL-1β and TNF diminishes PDAC CXCL5 secretion

To evaluate the effect of hAT-CM associated IL-1β and TNF on PDAC cells, we applied recombinant ligands to stimulate CXCL5 secretion of Panc1 cells. The Panc1 cells specifically had undetectable levels of either IL-1β or TNF in the RNA-seq analysis and were one of the lowest expressing cell lines of endogenous IL-1β, TNF, or CXCL5 according to the DepMap portal (online supplemental figure 2D,E); this led us to focus on the Panc1 cell line to eliminate autocrine effects outside of the hAT-CM contributing to CXCL5 release. ELISA of CXCL5 demonstrated both recombinant IL-1β or TNF are capable of inducing CXCL5 secretion (figure 3B). When assessing blocking antibodies in hAT-CM, individual neutralization failed to suppress CXCL5 secretion. Reduced CXCL5 secretion was only observed by combining IL-1β and TNF neutralizing antibodies, providing a significant suppressive effect against the pooled hAT-CM.

CXCL5-deficient PDAC shows non-differential growth but affects tumor-associated myeloid profiles

To assess the contribution of CXCL5 on PDAC tumor progression, we genetically depleted CXCL5 by CRISPR-Cas9: murine K8484-PDAC cells (KPC) were transfected for Cas9 expression, then subsequently with control (non-targeting control: NTC) or CXCL5 guide-RNAs. Positive clones from each guide RNA were validated for knockout by qPCR analysis (figure 4A). Control and knockout tumor cell proliferation differences were assessed by EdU incorporation. We found no deleterious effect of the knockout toward tumor growth from pooled clones of the same guide RNA (figure 4B); however, there was a slight but significant reduction in EdU incorporation of clone 3–17 when separately compared with the control (online supplemental figure 4A). To overcome
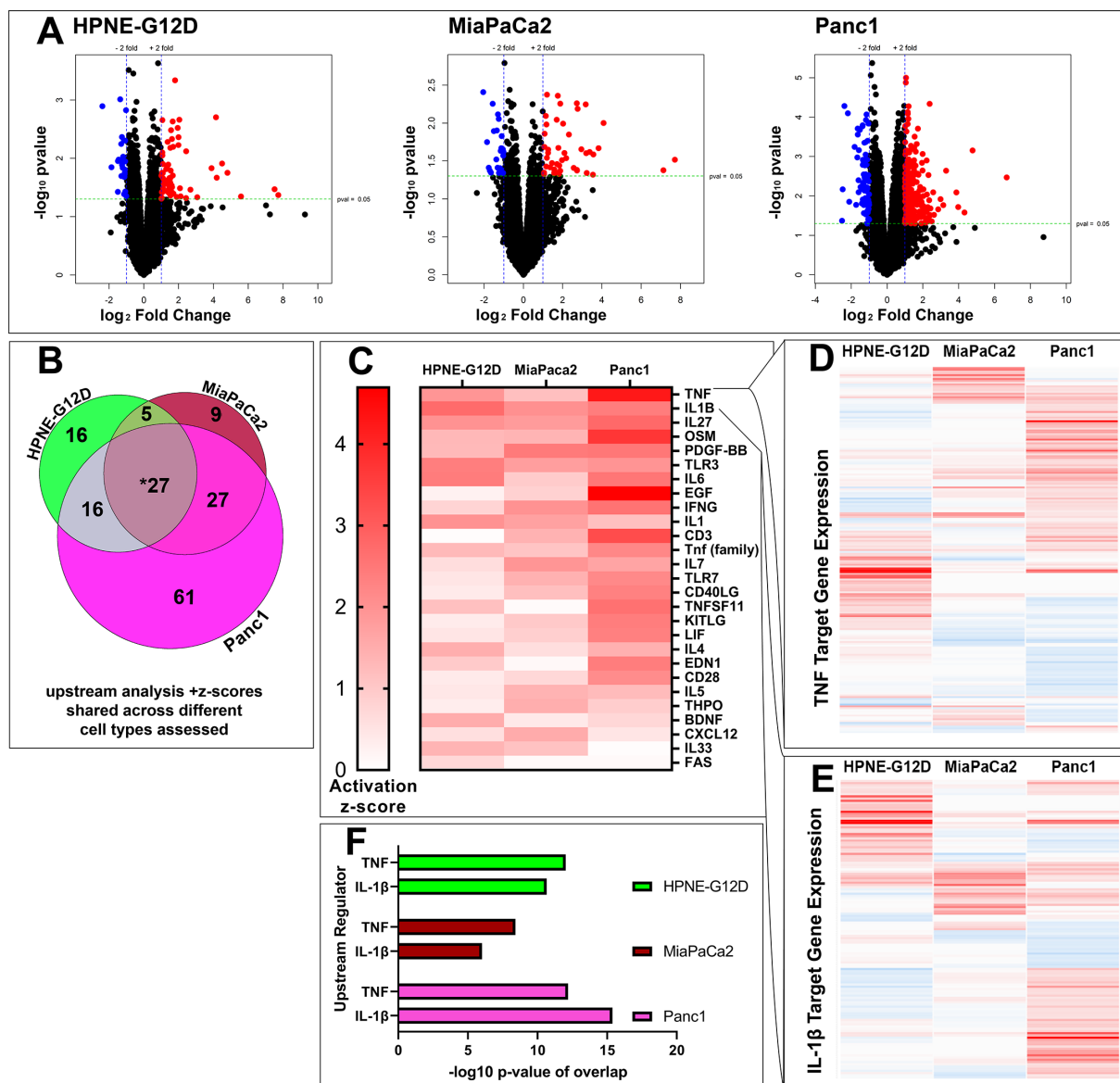
Figure 2 Eight individual **hAT-CM samples (four male, three female, and one non-reported sex of varying BMIs/stages, see online supplemental table 1) or two replicates of serum-free media were applied to the indicated cells in separate wells in cell culture in six well plates. RNA was isolated from each well and subjected to RNA sequencing analysis to assess the response of HPNE-G12D, Panc1, and MiaPaCa2 cells to hAT-CM (n=8, diluted 1:3 in serum-free media) versus serum-free conditions (n=2). (A) Volcano plots displaying differential gene expression in response to hAT-CM treatment across three cell lines: HPNE-G12D, Panc1, and MiaPaCa2, versus serum-free incubation. (B) Differentially expressed genes were subjected to Upstream Analysis using Qiagen Ingenuity Pathway Analysis (IPA); IPA was used to predict upstream signaling pathways (cytokines, growth factors, receptors) activated across all three cell lines tested in response to hAT-CM. The z-scores of the 27 (*) overlapping signaling pathways with positive z-scores, indicating potential influence on the cellular transcriptomes, were plotted in a heatmap in order of clustering in IPA (C). The top two hits (TNF and IL-1β) are expanded out (D, E) to visualize averaged $\log_2$FC versus serum free conditions for all genes associated with the pathway and their differential expression across cell lines in a heatmap clustered by Clustergrammer (see online supplemental figure 2C for permanent links to interactive plots prepared using Average linkage and Cosine distance, and online supplemental table 3 for the gene list/values input into Clustergrammer); Red=positive FC, Blue=Negative FC. Range for (D)=−2.38:7.73 across 200 pathway associated genes, (E)=−1.86:7.73 across 136 IL-1β associated genes. 94 genes overlap across both groups. (F) P values of TNF and IL-1β upstream pathway activity from IPA are plotted for each cell line. **6/8 samples received no neoadjuvant therapy, while 2/8 were not reported or treatment history was not found. Abbreviations: BMI, body mass index; hAT-CM, human adipose tissue conditioned media; IPA, ingenuity pathway analysis.

potential clonal differences, knockout clones from each guide RNA were mixed for tumor studies. Cells were orthotopically injected into the pancreas of obese, syngeneic Jax/B6 mice to assess effects on tumor growth and

immune infiltration (figure 4C). Tumor mass at endpoint failed to reveal an effect of CXCL5-knockout (figure 4D). Because of CXCL5's role in myeloid migration,[23 27] we looked for differences in myeloid immune infiltration
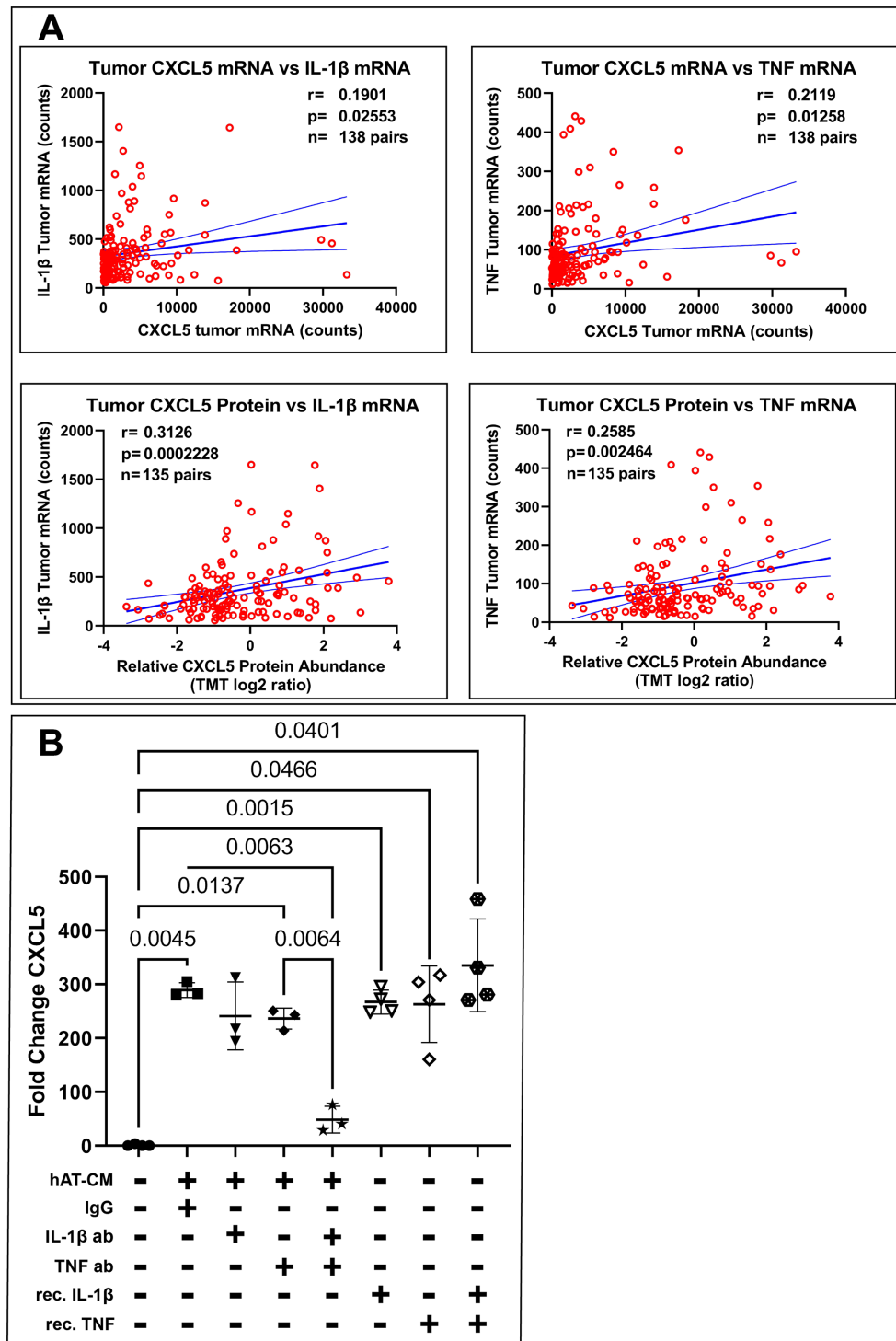
Figure 3 (A) RNA and protein data accessed from cProSite (platform for accessing NCI CPTAC and ICPC data derived from Proteomic Data Commons) were used to plot Pearson correlation of IL-1β mRNA (left) or TNF (right) mRNA with CXCL5. IL-1β and TNF mRNA were plotted against CXCL5 mRNA expression (top) or protein abundance (bottom) to show correlation of CXCL5 expression and abundance. IL-1β and TNF were not detected at the protein level; therefore, only mRNA was used for correlation analysis against CXCL5 expression or abundance. Data were analyzed in GraphPad Prism using the Simple linear regression function to calculate r and p values using Pearson correlation. (B) hAT-CM of pooled obese samples (BMI≥30; see online supplemental table 1 for associated samples and patient information) or recombinant IL-1β, TNF, or combo (1 μg/mL each) was used to stimulate CXCL5 release. Neutralizing antibodies against IL-1β or TNF were applied at 1 μg/mL to inhibit CXCL5 secretion in the presence of hAT-CM. Each treated group of Panc1 cells was treated for 36 hours and tumor conditioned media was collected, spun to remove cells, and CXCL5 levels secreted into the media were measured by ELISA. Statistics for (B) were performed by Brown-Forsythe and Welch's one way ANOVA, and only significant p values are displayed. n=3 for hAT-CM treated groups. n=4 for recombinant protein stimulus groups. (A) Error bars represent 95% CI and (B) error bars represent ±SD. ANOVA, analysis of variance; BMI, body mass index; hAT-CM, human adipose tissue conditioned media.
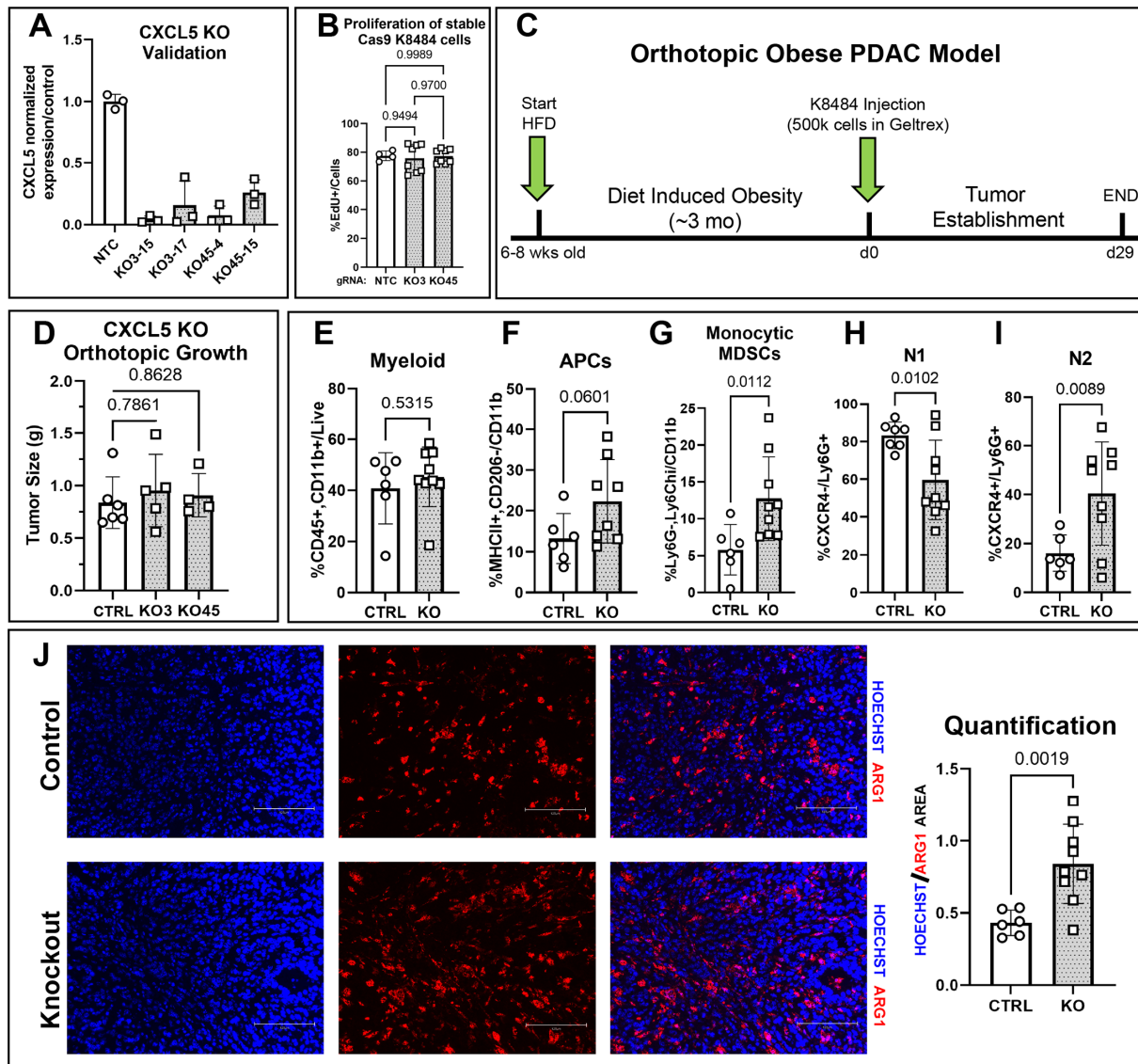
Figure 4 (A) Depletion of tumor CXCL5 was validated in murine Pancreatic Ductal Adenocarcinoma (PDAC) cell lines (K8484-KPC) by qPCR and normalized to non-targeting control guide RNA (NTC) levels. (B) Proliferation of the cells *in vitro* was measured by EdU incorporation over a 6-hour time period in 5% FBS DMEM (n=4 for NTC; 8/gRNA=2*4/clone). (C) *In vivo* study timeline: the Cas9+non-targeting control guide RNA carrying cells (CTRL) or pooled knockout clones (3–15+3-17: KO3), or (45–4+45-15: KO45) were then orthotopically injected (500k total cells in 50 µL Geltrex/injection) into the pancreas of syngeneic Jax/B6 mice maintained on high-fat/Western style diet for a minimum of 3 months. Tumors were allowed to grow for 29 days prior to takedown. Tumors were assessed for tumor mass in grams (D) and live (Live Dead stain negative) cells were assessed for myeloid (CD11b+) immune markers by flow cytometry (E–I): CD206-/MHCII+cells were considered potential antigen-presenting cells (APCs) from the LiveDead-/CD11b+positive population. Ly6G-, Ly6Chi CD11b+cells were considered potential monocytic myeloid-derived suppressor cells (MDSCs) from the LiveDead-/CD11b+population. CXCR4+ and CXCR4− events from Ly6G/CD11b+/LiveDead− cells were considered potential N1 and N2 neutrophils, respectively. Immunofluorescent staining of formalin-fixed paraffin-embedded tumor tissue sections for Arginase I (ARG1, red) counterstained with Hoechst nuclear dye (blue) was used to mark and quantify relative ARG1 abundance (ARG1+area/Hoechst area quantified in ImageJ) by microscopy at (imaged at 20×: scale bars represent 125 µm) indicating immunosuppressive stromal elements (J). Representative images of control (top) and knockout tumors (bottom) for quantification (right); three images were taken per tumor and averaged to provide values for quantification for each individual tumor plotted (n=6 CTRL, n=9 KO). Statistics were performed by Brown-Forsythe and Welch's one way ANOVA (B, D), or unpaired t-test with Welch's corrections in GraphPad Prism (E–J). Error bars are displayed as ±SD. ANOVA, analysis of variance; FBS, fetal bovine serum.

by flow cytometry. We observed no difference in gross myeloid (CD11b+) immune infiltration (figure 4E), but there was an insignificant trend toward increased number of antigen-presenting cells (APCs:MHCII+,CD206−/ CD11b+) (figure 4F). Specifically, we assessed for potential dendritic cells by staining for CD11c: we also observed an insignificant trend toward an increase in CD11c abundance histologically (online supplemental figure 4G).

Contrary to the anticipated results, we observed a drastic increase in the presumed monocytic MDSC (Ly6G–, Ly6Chi/CD11b+) population in our CXCL5-KO tumors (figure 4G). Using CXCR4 as a protumor, N2-neutrophil marker,[52] we observed neutrophil polarization to an N2 phenotype (figure 4H,I). Due to the potentially immune suppressive phenotype observed, we assessed ARG1 levels as a marker of immune suppression[53 54] by immunofluorescent staining, revealing significantly increased ARG1 in CXCL5KO tumors per nuclear area.

Loss of CXCL5 enhances CD8 T cell tumor infiltration and alters systemic CD8 memory profiles

While the neutrophil and MDSC profiles and immuno-suppressive arginase abundance of the CXCL5-knockout tumors were less favorable tumor phenotypes, we noted a population of CD45+cells that were CD11b negative during myeloid assessment (figure 5A): investigation of the CD3 profile of knockout tumors trended toward a favorable immune landscape: the CXCL5-knockout tumors revealed an increase in CD3 infiltration (figure 5B) in both CD4 and CD8 T cells (figure 5C), but this did not significantly increase the ratio of CD8:CD4 cells (figure 5C). Central memory CD8 T cells (CD62L+, CD44+/CD8) were increased in tumors (figure 5E) and spleens (figure 5F) of CXCL5-KO bearing mice. Central memory CD4 cells were also significantly increased in tumors and spleens of CXCL5KO tumor-bearing mice (online supplemental figure 5A,B), at the expense of effector CD4 cells, which were significantly reduced. Importantly, the CXCL5-KO tumor-bearing mice CD8 T cells displayed high PD-1 positivity, increased from the control tumors, and even present on circulating CD8+cells in the spleens (figure 5G). Tumor infiltrating CD4 cell PD-1 levels were not different between groups but were elevated in spleens of CXCL5-KO tumor-bearing mice.

CXCL5-deficient PDAC is susceptible to anti-PD1 immune checkpoint blockade therapy

Because CD8+cells in the CXCL5-KO tumors displayed substantial PD-1 positivity (figure 5G), we hypothesized that CBI therapy could provide a benefit in the CXCL5-deficient tumor setting. NTC and CXCL5-KO tumors were treated with an anti-PD-1 antibody therapy regimen[47] (figure 6A). Administration of the anti-PD-1 therapy led to a significant reduction of pancreatic mass in obese mice bearing CXCL5-KO tumors, while the same therapy provided no effect in the control group (figure 6B).

DISCUSSION

In this study, genetic ablation of tumor-derived CXCL5 in an obese mouse model prompted substantial infiltration of T cells into the TME, yet the tumors failed to display evidence of benefit due to exhaustion and suppressive immune phenotypes, but were susceptible to CBI.

IL-1β and TNF are cytokines shown to be released by adipose depots, with increased release in adipose and systemically from patients with higher BMI/obesity status.[51] We failed to see a significant difference in these cytokines in hAT-CM comparing overweight/obese PDAC patients to leaner patients; however, the power of this study was limited by the number and quantity of adipose, specifically from lean patients, and differential staging/disease progression, or contributions due to sex differences (online supplemental table 1). All samples were cancer-associated, and studies assessing alterations in adipose adipokine production between non-tumor-bearing and cancer patients have yet to be addressed. The implications of adipokine-tumor crosstalk have been previously investigated intrinsically through measuring tumor proliferation, metabolism, and migration;[40 55 56] we observed that TNF or IL-1β can induce the secretion of immune modulating CXCL5 from PDAC cells.

Further assessment shows TNF or IL-1β are sufficient for CXCL5 secretion. TNF can promote CXCL5 expression via CREB activation, which can be sourced from tumor-associated neutrophils (TANs);[18] however, endogenous TNF and CXCL5 expression in PDAC cell lines strongly correlate, while IL-1β does not (online supplemental figure 2D,E). Therefore, TNF may be sourced in an autocrine fashion by tumor cells, paracrine from CAFs, by tumor-associated macrophages, and we speculate that endocrine/paracrine sources from adipose tissue could systemically increase TNF in an in vivo context, as has been evidenced by adipose-derived IL-1β on blood glucose levels.[57] Concordantly, obese mice have enhanced TAN infiltration driven by IL-1β[6 58]: depletion of TANs reduces CXCL1 levels but does not ablate them,[6] suggesting that other factors drive CXCL1 secretion supplementing TAN-sourced TNF.[18] Whether the evidence of obesity and IL-1β driven TAN infiltration is directly due to adipose remains to be elucidated.

IL-1β and TNF both contribute to CXCL5 secretion via the NF-kB pathway in inflammatory contexts.[27 59] Our results show that the presence of either TNF or IL-1β appears sufficient to promote CXCL5 release from cancer cells, while only blockade of both limited secretion of CXCL5 in our *in vitro* approach in a cell line that expresses lower levels of each (figure 3, online supplemental figure S2D,E). IL-1β alone has been evidenced to be sufficient for stimulating mRNA expression of CXCL1 and CXCL2 human PDAC cell lines.[60] A recent study investigating TME ligand and cancer cell intrinsic response by single-cell RNA sequencing revealed IL-1A, HGF, IL-15, and IL-17A induced a similar NF-kB pathway induction to TNF/IL-1β, which warrants further investigation in the regulation of tumor CXCL release.[61] Notably, fatty acids from adipose (palmitate) can induce CXCR1/2 ligand secretion from hepatocellular carcinoma cells.[62] This could contribute to residual secretion after combination blockade of IL-1β/TNF *in vitro*. Additionally, tumor-associated macrophages may also contribute TGFβ1 and
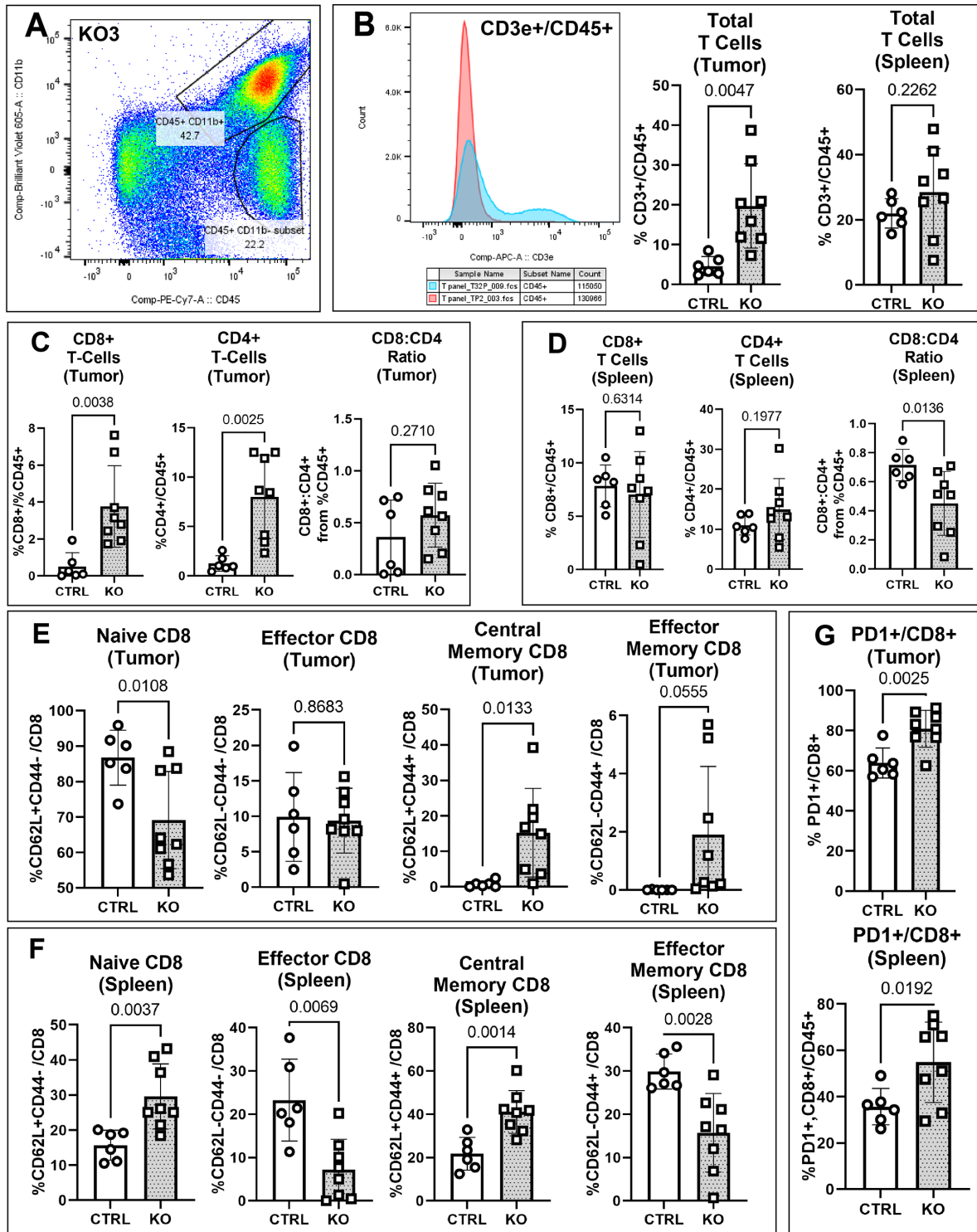
Figure 5 (A) Representative FlowJo plot of CD11b (y-axis) versus CD45 (x-axis) staining from CXCL5KO tumor depicting CD11b− CD45+ population of interest. (B) Cells were gated for CD45 positivity then plotted for CD3 positivity: Representative histogram of CD3 staining in CXCL5KO (T32P, tumor KO3, number 2, blue) tumor versus control (TP2, red) and quantification of CD3+cells as percentage of CD45+cells in tumors shows significantly greater CD3 T cell infiltration in CXCL5KO tumors (middle), but no difference in spleen abundance (right) of mice bearing control or CXCL5KO KPC tumors. Quantification of CD8+ or CD4+ cells as a percentage of CD45+Live cells (gated prior for negative Live/Dead stain and CD45 positivity) shows an increase in CXCL5KO tumors (C) but not spleens (D). CD8 polarization is shown as naïve, effector, central memory, or effector memory CD8 T cells from tumor (E) or spleens (F) distinguished by CD62L and CD44 axes: central memory CD8 T cells (CD62L+CD44+) are increased in CXCL5KO tumor-bearing mice in both tumors and spleens. PD1 positivity of the CD8+ population of T cells is greater in tumors (top) and spleens (bottom) of CXCL5KO tumor-bearing mice compared with control (G). (n=6 CTRL, n=8 KO) Statistics: Unpaired T-test with Welch's corrections in GraphPad Prism (E–J). Error bars are displayed as ±SD.
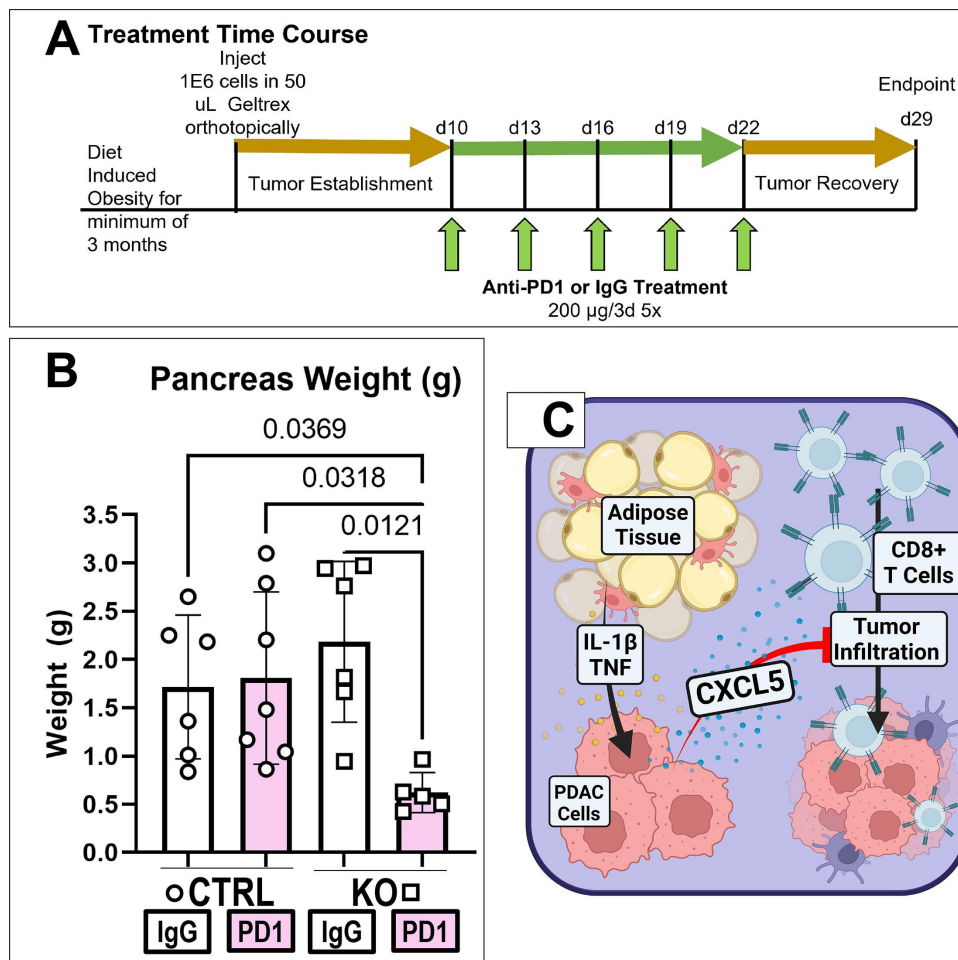
Figure 6 (A) Schematic depicting study timeline: Syngeneic, Jax/B6 mice were fed a high-fat/Western style diet to drive diet-induced obesity for a minimum of 3 months, then were orthotopically injected with either 1E6 Cas9+non-targeting control guide RNA ("CTRL") or a 50/50 mix of Cas9+CXCL5 knockout clones 3–15 and 3–17 ("KO") K8484-KPC cells, similar to figure 4B, resuspended in 50 μL Geltrex per injection. At day 10 post-tumor implantation, mice were treated with 200 μg in 100 μL volume of anti-PD-1 antibody (Clone 29F1A12) or IgG (Clone 2A3) diluted in *InVivo*Pure pH 7.0 dilution buffer and continued every third day until day 22. Whole pancreas+tumor mass (g) was assessed at endpoint (d29) revealing statistically significant reduction in tumor mass only in KO tumors treated with anti-PD-1 therapy (B). Statistics were performed by Brown-Forsythe and Welch's one way ANOVA, and all significant ($p<0.05$) p values are shown and considered significant; error bars are displayed as ±SD. n=5–6 per group. (C) Illustrative representation of study: Adipose tissue explants contain cytokines from adipocytes or monocytes that can stimulate CXCL5 release from Pancreatic Ductal Adenocarcinoma (PDAC) cells *in vitro*; CXCL5 acts as a critical deterrent to tumor T cell infiltration in in vivo studies where CXCL5 depletion permits intratumoral T cell infiltration. Illustration created in BioRender: Walsh (2024) https://BioRender.com/h45s779. ANOVA, analysis of variance.

PDGFβ to the microenvironment in obese tumors, which could contribute to these axes via CAF differentiation.[5 63]

TCGA analysis shows CXCL5 significantly correlates with survival separated at median expression, corroborating other studies referencing TCGA data (dataset).[19 36 48] Yet, Steele *et al* showed in analyses of biopsies from resected tumors that CXCL2 is associated with worsened patient outcome;[23 27] the survival trend was observed in our analysis, while statistically insignificant (online supplemental figure 1B, p=0.13). This may change with staging distributions in assessed populations, as we saw a trend toward a stage-dependent increase of CXCL5 as previously reported[20] but did not investigate other chemokines.

Higher ARG1 expression is associated with worsened patient outcomes in PDAC patients; additionally, it has

been reported to be predominantly derived through the myeloid population in GEM models of PDAC, but a subpopulation of Ly6C+CD8+T cells also displayed ARG1 expression.[34 53 54] With the increase of intratumoral CD8+T cells into CXCL5 KO tumors, we suspect that this subpopulation of cells may be contributing to the increased ARG1 observed by immunofluorescence, although the presence of this population of T cells appears to be dependent on epithelial KRAS inactivation.[34]

Furthermore, while we saw an insignificant trend toward more MHCII+APCs in the CXCL5-knockout tumors (figure 4F), we did not see a difference in CD11b+/iNOS+cells histologically, a marker for M1-like macrophages which have been shown to be critical for CBI immunotherapy efficacy.[14 64] However, iNOS was detected

in the myeloid population, which can drive MDSC recruitment observed in both knockout and control tumors.[65] We suspect a window of opportunity to observe such a difference in iNOS may have passed by the time of tumor collection, with the MDSC population already recruited. Additionally, we speculate that iNOS:CXCL5 ratios in the tumors may contribute toward the monocytic MDSC infiltration, but this requires further investigation.

CXCL5KO lung tumors were shown to increase T cell effector-memory cells compared with controls, regulated by differential neutrophil recruitment in CXCL5KO versus WT tumors.[37] While we did not observe a significant increase in effector-memory CD8s (CD62L–/CD44hi), we did see an increase in central memory T cells present in both the CD8 and CD4 populations (figure 5E, online supplemental figure 5A). Further investigation into the role of tumor-derived CXCL5 versus obesity factors influencing myeloid infiltration may elucidate whether these conflicting observations are due to cancer-type context,[66] stromal factors of obesity models,[6] differences in experiment timing (end-point vs establishment), or artifacts of fluorescent peptide uptake by APCs.[67 68]

The role of CXC ligands in tumor immune regulation is being extensively investigated, providing many promising therapeutic opportunities, but individual ligands are now being further defined with differentiating properties and effects. Other CXCR1/2 ligands include CXCL1, CXCL2, CXCL8; broad spectrum CXCR1/2 inhibition has been shown to enhance CD8 T cell-mediated alleviation of tumor burden.[22 23 69] CXCL8 has been shown to be detectable in the serum of a subset of PDAC patients and has clinical predictive capacity with CXCL8+patients displaying worsened survival outcomes.[70] While CAFs are a profound contributor to intratumoral CXCL8 (IL-8), tumor-associated myeloid immune cells, and cancer cells themselves also contribute to these levels: CXCL8 acts in both an autocrine and paracrine fashion across tumor constituents, driving stemness and migratory properties in cancer cells, angiogenesis, and impeding T-cell function.[25 71–74] Further, angiogenesis has been shown to be driven in a VEGF-independent manner via PDAC CXCL1, CXCL5, and CXCL8 expression.[75 76] In the context of another CXCR1/2 ligand, CXCL2, a recent study revealed that both CXCL2 and CXCL5 expression is increased via YAP1 activity in stressed tumor cells, and either chemokine is capable of inducing mTORC activation in CAFs and pro-tumorigenic neutrophil-extracellular-trap formation in neutrophils.[77 78] A study using multiple cancer models, including PDAC, concluded that cancer cell expression of PD-L2 is essential for CXCL1 and CXCL2 expression, which promotes immune evasive myeloid profiles.[79] Further, in a model of hepatocellular carcinoma, tumor-derived CXCL2 has been shown to enhance TAN CCL4 expression, promoting CD155 expression in cancer cells that allows for evasion of CD8-mediated cell killing.[80]

CXCR2 ligands, including CXCL5, are evidenced to enhance pro-tumor myeloid cells to the PDAC-TME.[18 23 27 31 36] Despite canonical CXCR1/2 ligand myeloid trafficking, our CXCL5-KO tumors displayed an unexpected enrichment of Ly6Chi, Ly6G–/CD11b+ cells resembling monocytic-MDSCs (figure 4G), as well as an immunosuppressive increase in ARG1 (figure 4J) which would explain the lack of tumor burden difference in CXCL5KO tumor-bearing mice and susceptibility to PD-1 inhibition.[14] Alternatively, a model of CXCR2 heterozygous knockout in a PDAC GEM model reduced ARG1+tumor-associated macrophages in the TME.[24] This suggests that there may be differential effects of related CXC-ligands, with specific subtleties in targets and effects. The individual effects of each CXCL would be important to investigate in future studies, and whether compounding both CXCL1/5 targeting is differentially beneficial than either alone. Considering CXCR1/2 blockade in patients is being investigated, CXCL1 ablation has been shown to reduce tumor volume without the need for immunotherapeutic intervention preclinically[18 26]; therefore, CXCL5 may be a less critical target as depletion of CXCL5 required immune therapy application to reduce tumor burden in our study and may impede effects of CXCR1/2 inhibition compared with targeting CXCL1 alone.

CXCL1 is implicated as a critical regulator of T cell infiltration, which is expressed through TNF-mediated CREB signaling and can be abrogated via combined MEK and STAT3 inhibition.[18 81] Our data suggest that CXCL5 loss specifically leads to a tumor suppressive myeloid profile in contrast to CXCL1 loss, with the caveat that an obese TME may contribute to the discrepancy.[6] Furthermore, CXCL5 overexpression in an orthotopic KRC (Kras$^{G12D/+}$, Rnf43$^{-/-}$) model enhanced tumor progression by restoring mutant Kras-associated immune phenotypes.[82] To elicit an antitumor effect, CXCL5 depletion requires CBI for an antitumor response in a manner similar to CXCL8 (IL-8),[18 25] which was reflected in a study showing HDAC activity silences CXCL5 expression, promoting an immunologically unique microenvironment.[82] In contrast, CXCR2-ligand signaling affects autonomous proliferation both negatively and positively in the following studies: Application of recombinant CXCL1 in vitro to ductal cells induced senescence,[83] yet CXCR2-knockdown inhibits PDAC cell growth;[33] additionally, CXCL1 autocrine signaling promotes proliferation of esophageal cancer cells.[84] Our analysis of CXCL5-knockout cells displayed no observed effect on tumor cell proliferation among three of the four clonal populations (online supplemental figure 4A), nor did we see differential tumor mass in vivo (figure 4D), despite evidence of CXCR2 being a regulator of intrinsic tumor cell proliferation.[33 85]

Our studies have uncovered potential expanded functions of CXCL5 for further consideration. Interestingly, CXCL1 and CXCL5 have been shown to interact by immunoligand blotting[86] and are predicted to interact in silico[87] (online supplemental figure 6) in a heterodimer that appears similar to homodimer CXCL5;[88] dimerized CXCL1 has been shown to enhance CXCR1 activation.[89]

Perhaps CXCL5 loss in our studies reduces CXCL1/5 interaction that potentiates CXCL1-mediated chemotaxis of the monocytic MDSCs into the tumor. Yet the function of the CXC-ligand dimerizations requires further investigation to determine whether CXCL1/5 homo/heterodimers have differential effects on CXCR1/2. Alternatively, a potential contribution of the adipokines to promote MAPK activation in an obese setting was noted from the RNAseq analysis, which may contribute to the PD-1/PD-L1 axis, supplemental to dependence on the myeloid population.[14]

Clinically, we speculate that targeting CXCL5 alone would be less beneficial at improving the TME in patients than targeting multiple chemokines (CXCL1, CXCL8, etc) when combined with checkpoint blockade. Specifically, preclinical studies targeting CXCL1 did not require CBI to elicit antitumor effects,[18] whereas we demonstrate that CXCL5 depletion in our model does require CBI. As TNF drives expression of both CXCL1 and CXCL5 in PDAC cells, therefore, repurposing of FDA-approved TNF blockers in PDAC may be beneficial to increase CBI efficacy in PDAC patients. While obese humans typically have higher circulating TNF levels due to adiposity, it is unclear whether this is present in patients with cancer. Therefore, it may be beneficial to consider TNF levels in PDAC patients versus non-tumor-bearing obese and lean patients to assess whether this strategy would be specific to obese patients. Targeting of CXCL5 requires further investigation; some possibilities would include direct genetic targeting or indirect pharmacologic targeting. Direct targeting of CXCL5 via RNA interference may be possible, as RNA interference of targeted molecules in other cancers has shown efficacy, and a phase 0 study of siKRAS in PDAC patients has been reported safe.[90 91] Alternatively, we are pursuing an adeno-associated viral mediated tumor-specific delivery of siRNA. Indirect targeting via CXCR1/2 inhibitors is under clinical investigation; yet, it has been reported that CXCR2-KO mice are more susceptible to lung infections, thus broad-spectrum CXCR targeting may have adverse effects in patients at higher risk for respiratory tract infections, such as obese patients.[92 93] Whether the increased risk of respiratory infection in obese patients would compound with CXCR inhibition would be important to consider before clinical implementation. We suspect that interventions targeting CXCL5 should precede CBI intervention in future clinical applications in order to create a TME permissive to additional therapies. Monitoring response efficacy via biomarkers should include assessment of circulating T cells for PD-1 positivity as an exhaustion marker, but also activation marker. Prior to implementation, CXCL5 levels as well as CXCL1, CXCL8, TNF and IL-1β should also be measured before implementing therapeutic strategies that target any of them.

In conclusion, our studies highlight the role for tumor-derived CXCL5 in regulating an antitumor immune response. While the exact mechanism is still unclear, our results suggest that depletion of CXCL5 in the setting of obesity is sufficient to induce CD8 T cell infiltration into pancreatic tumors. Loss of tumor-derived CXCL5 increases immune suppression via increased myeloid cell recruitment and polarization. Therefore, depletion of CXCL5 requires anti-PD-1 therapy to achieve suppression of pancreatic cancer growth.

These studies supplement previous research into CXC-ligand family proteins by suggesting CXCL5 plays an alternative role in PDAC immune recruitment to other CXCLs and emphasizes that depletion of at least CXCL5 can be effective and beneficial even in the context of obesity, although requiring supplemental checkpoint blockade intervention. Given that TNF appears to be a predominant driving factor in CXCR ligand expression, the combination of CXCR1/2 inhibitors and TNF/IL-1β blockers in PDAC patients may increase efficacy, particularly in cases where TNF/IL-1β are reportedly elevated systemically, such as in obesity.

Limitations

Limitations to this study include the lack of lean control and CXCL5KO tumor-bearing tumors. Whether the role of tumor-derived CXCL5 on increasing the immunosuppressive MDSC population or intratumoral ARG1 has yet to be investigated in the context of an obese mouse model. Differences observed in the knockout of PDAC CXCL5 from this study compared with effects seen from CXCL1 ablation in other studies may not be as severe in lean tumor-bearing mice, as our obese model may be driving other immunosuppressive phenotypes in the TME.[6 18 58] Further, this study did not account for changes to the CAF population that could be affected by alterations to CXCL5 or the context of obesity, as IL-1β has been shown to induce antigen-presenting CAF differentiation from mesothelial cells, which can contribute to immune suppression.[63 94] Further, comparison of phenotypes in response to depletion of other CXCR1/2 ligands was not performed in this study. Future studies expanding on specific subtleties of depleting individual chemokines, particularly in myeloid infiltration, would be of great interest to us and other researchers. Further immune profiling of tumors histologically in this study was limited by cross-reactivity of antibodies, and we, therefore, could not assess cell of origin for ARG1 abundance in tissue sections. Future studies should include a more intensive immune-profiling panel, specifically looking at potential dendritic cell and natural killer cell involvement in response to CXCL5 depletion.

Patient samples were limited based on availability. Information on sex/age is missing for 4/19 patient samples, one of which was included in the RNAseq data set (online supplemental table 1). Additionally, there was no reporting of therapy for these patients, and one additional patient used in pooled CM experiments. Only one patient within this study was reported to receive neoadjuvant therapy; this sample was only used in the assessment of TNF/IL-1B from conditioned media (online supplemental figure 2B), but no other

experiments. Inclusion criteria for sample selection were based on a positive diagnosis of pancreatic adenocarcinoma; samples were processed and allocated for use in the study based on whether the mass of the sample was enough to generate conditioned media. Future studies assessing PDAC response to hAT-CM samples based on the sex of the patients may be insightful in identifying whether there are inherent differences in female versus male tumor-associated adipose; however, the limited number of samples (n=4 male, 3 female) failed to yield consistent, significant results across cell lines. This may be due to the range of staging across the samples or other confounding factors. Due to the limited mass of adipose from lean patients, it was difficult to assess properties of hAT-CM across multiple assays using the same samples, and therefore, make conclusive comparisons across BMI status or sex.

X Richard McKinnon Walsh @mckinnon_walsh, Austin E Eades @AwEades, Bailey A Bye @Bailey__Bye, Mariana Tannus Ruckert @ruckertmt and Michael N VanSaun @MichaelVansaun

ORCID iDs
Richard McKinnon Walsh http://orcid.org/0000-0003-2338-3115
Austin E Eades http://orcid.org/0000-0002-1790-8301
Mariana Tannus Ruckert http://orcid.org/0000-0002-8282-4454
Prabhakar Chalise http://orcid.org/0000-0001-5581-1220
Michael N VanSaun http://orcid.org/0000-0002-2538-8107

REFERENCES

1. Rahib L, Wehner MR, Matrisian LM, *et al*. Estimated Projection of US Cancer Incidence and Death to 2040. *JAMA Netw Open* 2021;4:e214708.
2. Arslan AA, Helzlsouer KJ, Kooperberg C, *et al*. Anthropometric measures, body mass index, and pancreatic cancer: a pooled analysis from the Pancreatic Cancer Cohort Consortium (PanScan). *Arch Intern Med* 2010;170:791–802.
3. Li D, Morris JS, Liu J, *et al*. Body mass index and risk, age of onset, and survival in patients with pancreatic cancer. *JAMA* 2009;301:2553–62.
4. VanSaun MN, Lee IK, Washington MK, *et al*. High fat diet induced hepatic steatosis establishes a permissive microenvironment for colorectal metastases and promotes primary dysplasia in a murine model. *Am J Pathol* 2009;175:355–64.
5. Chung KM, Singh J, Lawres L, *et al*. Endocrine-Exocrine Signaling Drives Obesity-Associated Pancreatic Ductal Adenocarcinoma. *Cell* 2020;181:832–47.
6. Incio J, Liu H, Suboj P, *et al*. Obesity-Induced Inflammation and Desmoplasia Promote Pancreatic Cancer Progression and Resistance to Chemotherapy. *Cancer Discov* 2016;6:852–69.
7. Philip B, Roland CL, Daniluk J, *et al*. A high-fat diet activates oncogenic Kras and COX2 to induce development of pancreatic ductal adenocarcinoma in mice. *Gastroenterology* 2013;145:1449–58.
8. Calle EE, Rodriguez C, Walker-Thurmond K, *et al*. Overweight, obesity, and mortality from cancer in a prospectively studied cohort of U.S. adults. *N Engl J Med* 2003;348:1625–38.
9. Vansaun MN. Molecular pathways: adiponectin and leptin signaling in cancer. *Clin Cancer Res* 2013;19:1926–32.
10. Mendonsa AM, Chalfant MC, Gorden LD, *et al*. Modulation of the leptin receptor mediates tumor growth and migration of pancreatic cancer cells. *PLoS One* 2015;10:e0126686.

11 Schäffler A, Schölmerich J, Buechler C. Mechanisms of disease: adipokines and breast cancer - endocrine and paracrine mechanisms that connect adiposity and breast cancer. *Nat Clin Pract Endocrinol Metab* 2007;3:345–54.

12 Holowatyj AN, Haffa M, Lin T, *et al*. Multi-omics Analysis Reveals Adipose-tumor Crosstalk in Patients with Colorectal Cancer. *Cancer Prev Res (Phila)* 2020;13:817–28.

13 Rupert JE, Narasimhan A, Jengelley DHA, *et al*. Tumor-derived IL-6 and trans-signaling among tumor, fat, and muscle mediate pancreatic cancer cachexia. *J Exp Med* 2021;218:e20190450.

14 Zhang Y, Velez-Delgado A, Mathew E, *et al*. Myeloid cells are required for PD-1/PD-L1 checkpoint activation and the establishment of an immunosuppressive environment in pancreatic cancer. *Gut* 2017;66:124–36.

15 Sharma NS, Gupta VK, Garrido VT, *et al*. Targeting tumor-intrinsic hexosamine biosynthesis sensitizes pancreatic cancer to anti-PD1 therapy. *J Clin Invest* 2020;130:451–65.

16 Ma Y, Li J, Wang H, *et al*. Combination of PD-1 Inhibitor and OX40 Agonist Induces Tumor Rejection and Immune Memory in Mouse Models of Pancreatic Cancer. *Gastroenterology* 2020;159:306–19.

17 Doi T, Muro K, Ishii H, *et al*. A Phase I Study of the Anti-CC Chemokine Receptor 4 Antibody, Mogamulizumab, in Combination with Nivolumab in Patients with Advanced or Metastatic Solid Tumors. *Clin Cancer Res* 2019;25:6614–22.

18 Bianchi A, De Castro Silva I, Deshpande NU, *et al*. Cell-Autonomous Cxcl1 Sustains Tolerogenic Circuitries and Stromal Inflammation via Neutrophil-Derived TNF in Pancreatic Cancer. *Cancer Discov* 2023;13:1428–53.

19 Li A, King J, Moro A, *et al*. Overexpression of CXCL5 is associated with poor survival in patients with pancreatic cancer. *Am J Pathol* 2011;178:1340–9.

20 Saxena S, Molczyk C, Purohit A, *et al*. Differential expression profile of CXC-receptor-2 ligands as potential biomarkers in pancreatic ductal adenocarcinoma. *Am J Cancer Res* 2022;12:68–90.

21 Tang KH, Li S, Khodadadi - Jamayran A, *et al*. Combined inhibition of SHP2 and CXCR1/2 promotes anti-tumor T cell response in NSCLC. *Biorxiv* 2021. Available: https://www.biorxiv.org/content/10.1101/2021.03.21.436338v1.full.pdf

22 Piro G, Carbone C, Agostini A, *et al*. CXCR1/2 dual-inhibitor ladarixin reduces tumour burden and promotes immunotherapy response in pancreatic cancer. *Br J Cancer* 2023;128:331–41.

23 Steele CW, Karim SA, Leach JDG, *et al*. CXCR2 Inhibition Profoundly Suppresses Metastases and Augments Immunotherapy in Pancreatic Ductal Adenocarcinoma. *Cancer Cell* 2016;29:832–45.

24 Sano M, Ijichi H, Takahashi R, *et al*. Blocking CXCLs-CXCR2 axis in tumor-stromal interactions contributes to survival in a mouse model of pancreatic ductal adenocarcinoma through reduced cell invasion/migration and a shift of immune-inflammatory microenvironment. *Oncogenesis* 2019;8:8.

25 Li P, Rozich N, Wang J, *et al*. Anti-IL-8 antibody activates myeloid cells and potentiates the anti-tumor activity of anti-PD-1 antibody in the humanized pancreatic cancer murine model. *Cancer Lett* 2022;539:215722.

26 Li J, Byrne KT, Yan F, *et al*. Tumor Cell-Intrinsic Factors Underlie Heterogeneity of Immune Cell Infiltration and Response to Immunotherapy. *Immunity* 2018;49:178–93.

27 Chao T, Furth EE, Vonderheide RH. CXCR2-Dependent Accumulation of Tumor-Associated Neutrophils Regulates T-cell Immunity in Pancreatic Ductal Adenocarcinoma. *Cancer Immunol Res* 2016;4:968–82.

28 Zuo C, Baer JM, Knolhoff BL, *et al*. Stromal and therapy-induced macrophage proliferation promotes PDAC progression and susceptibility to innate immunotherapy. *J Exp Med* 2023;220:e20212062.

29 DeNardo DG, Ruffell B. Macrophages as regulators of tumour immunity and immunotherapy. *Nat Rev Immunol* 2019;19:369–82.

30 Carpenter ES, Kadiyala P, Elhossiny AM, *et al*. KRT17high/CXCL8+ Tumor Cells Display Both Classical and Basal Features and Regulate Myeloid Infiltration in the Pancreatic Cancer Microenvironment. *Clin Cancer Res* 2024;30:2497–513.

31 Nywening TM, Belt BA, Cullinan DR, *et al*. Targeting both tumour-associated CXCR2+ neutrophils and CCR2+ macrophages disrupts myeloid recruitment and improves chemotherapeutic responses in pancreatic ductal adenocarcinoma. *Gut* 2018;67:1112–23.

32 Liao C-Y, Li G, Kang F-P, *et al*. Necroptosis enhances "don't eat me" signal and induces macrophage extracellular traps to promote pancreatic cancer liver metastasis. *Nat Commun* 2024;15:6043.

33 Purohit A, Varney M, Rachagani S. CXCR2 signaling regulates KRAS(G12D)-induced autocrine growth of pancreatic cancer. *Oncotarget* 2016;7:7280–96.

34 Velez-Delgado A, Donahue KL, Brown KL, *et al*. Extrinsic KRAS Signaling Shapes the Pancreatic Microenvironment Through Fibroblast Reprogramming. *Cell Mol Gastroenterol Hepatol* 2022;13:1673–99.

35 Koltsova EK, Ley K. The mysterious ways of the chemokine CXCL5. *Immunity* 2010;33:7–9.

36 Zhang R, Liu Q, Peng J, *et al*. CXCL5 overexpression predicts a poor prognosis in pancreatic ductal adenocarcinoma and is correlated with immune cell infiltration. *J Cancer* 2020;11:2371–81.

37 Simoncello F, Piperno GM, Caronni N, *et al*. CXCL5-mediated accumulation of mature neutrophils in lung cancer tissues impairs the differentiation program of anticancer CD8 T cells and limits the efficacy of checkpoint inhibitors. *Oncoimmunology* 2022;11:2059876.

38 Olive KP, Jacobetz MA, Davidson CJ, *et al*. Inhibition of Hedgehog signaling enhances delivery of chemotherapy in a mouse model of pancreatic cancer. *Science* 2009;324:1457–61.

39 Kahn D, Macias E, Zarini S, *et al*. Exploring Visceral and Subcutaneous Adipose Tissue Secretomes in Human Obesity: Implications for Metabolic Disease. *Endocrinology* 2022;163:bqac140.

40 Manley SJ, Olou AA, Jack JL, *et al*. Synthetic adiponectin-receptor agonist, AdipoRon, induces glycolytic dependence in pancreatic cancer cells. *Cell Death Dis* 2022;13:114.

41 Zhang Y, Parmigiani G, Johnson WE. *ComBat-seq*: batch effect adjustment for RNA-seq count data. *NAR Genom Bioinform* 2020;2:lqaa078.

42 Li B, Dewey CN. RSEM: accurate transcript quantification from RNA-Seq data with or without a reference genome. *BMC Bioinformatics* 2011;12:323.

43 Langmead B, Salzberg SL. Fast gapped-read alignment with Bowtie 2. *Nat Methods* 2012;9:357–9.

44 Awaji M, Saxena S, Wu L, *et al*. CXCR2 signaling promotes secretory cancer-associated fibroblasts in pancreatic ductal adenocarcinoma. *FASEB J* 2020;34:9405–18.

45 Livak KJ, Schmittgen TD. Analysis of relative gene expression data using real-time quantitative PCR and the 2(-Delta Delta C(T)) Method. *Methods* 2001;25:402–8.

46 Ho TTB, Nasti A, Seki A, *et al*. Combination of gemcitabine and anti-PD-1 antibody enhances the anticancer effect of M1 macrophages and the Th1 response in a murine model of pancreatic cancer liver metastasis. *J Immunother Cancer* 2020;8:e001367.

47 Wang W, Marinis JM, Beal AM, *et al*. RIP1 Kinase Drives Macrophage-Mediated Adaptive Immune Tolerance in Pancreatic Cancer. *Cancer Cell* 2018;34:757–74.

48 Tang Z, Li C, Kang B, *et al*. GEPIA: a web server for cancer and normal gene expression profiling and interactive analyses. *Nucleic Acids Res* 2017;45:W98–102.

49 Wang D, Qian X, Du Y-C, *et al*. Abstract 3912: cProSite: a web based interactive platform for on-line proteomics and phosphoproteomics data analysis. *Cancer Res* 2022;82:3912.

50 Li Y, Dou Y, Da Veiga Leprevost F, *et al*. Proteogenomic data and resources for pan-cancer analysis. *Cancer Cell* 2023;41:1397–406.

51 Fain JN, Madan AK, Hiler ML, *et al*. Comparison of the release of adipokines by adipose tissue, adipose tissue matrix, and adipocytes from visceral and subcutaneous abdominal adipose tissues of obese humans. *Endocrinology* 2004;145:2273–82.

52 Peng Z, Liu C, Victor AR, *et al*. Tumors exploit CXCR4hiCD62Llo aged neutrophils to facilitate metastatic spread. *Oncoimmunology* 2021;10:1870811.

53 Menjivar RE, Nwosu ZC, Du W, *et al*. Arginase 1 is a key driver of immune suppression in pancreatic cancer. *Elife* 2023;12:e80721.

54 Apiz Saab JJ, Dzierozynski LN, Jonker PB, *et al*. Pancreatic tumors exhibit myeloid-driven amino acid stress and upregulate arginine biosynthesis. *Elife* 2023;12:e81289.

55 Messaggio F, Mendonsa AM, Castellanos J, *et al*. Adiponectin receptor agonists inhibit leptin induced pSTAT3 and *in vivo* pancreatic tumor growth. *Oncotarget* 2017;8:85378–91.

56 Pu X, Chen D. Targeting Adipokines in Obesity-Related Tumors. *Front Oncol* 2021;11:685923.

57 Nov O, Shapiro H, Ovadia H, *et al*. Interleukin-1β regulates fat-liver crosstalk in obesity by auto-paracrine modulation of adipose tissue inflammation and expandability. *PLoS One* 2013;8:e53626.

58 Incio J, Tam J, Rahbari NN, *et al*. PlGF/VEGFR-1 Signaling Promotes Macrophage Polarization and Accelerated Tumor Progression in Obesity. *Clin Cancer Res* 2016;22:2993–3004.

59 Friedrich M, Pohin M, Jackson MA, *et al*. IL-1-driven stromal-neutrophil interactions define a subset of patients with inflammatory bowel disease that does not respond to therapies. *Nat Med* 2021;27:1970–81.

60 Okabe J, Kodama T, Sato Y, *et al*. Regnase-1 downregulation promotes pancreatic cancer through myeloid-derived suppressor

cell-mediated evasion of anticancer immunity. *J Exp Clin Cancer Res* 2023;42:262.

61 Liu N, Kattan WE, Mead BE, *et al*. Scalable, compressed phenotypic screening using pooled perturbations. *Nat Biotechnol* 2024.

62 Dahlquist KJV, Voth LC, Fee AJ, *et al*. An Autocrine Role for CXCL1 in Progression of Hepatocellular Carcinoma. *Anticancer Res* 2020;40:6075–81.

63 Huang H, Wang Z, Zhang Y, *et al*. Mesothelial cell-derived antigen-presenting cancer-associated fibroblasts induce expansion of regulatory T cells in pancreatic cancer. *Cancer Cell* 2022;40:656–73.

64 van Elsas MJ, Middelburg J, Labrie C, *et al*. Immunotherapy-activated T cells recruit and skew late-stage activated M1-like macrophages that are critical for therapeutic efficacy. *Cancer Cell* 2024;42:1032–50.

65 Hanoteau A, Newton JM, Krupar R, *et al*. Tumor microenvironment modulation enhances immunologic benefit of chemoradiotherapy. *J Immunother Cancer* 2019;7:10.

66 Hegde S, Krisnawan VE, Herzog BH, *et al*. Dendritic Cell Paucity Leads to Dysfunctional Immune Surveillance in Pancreatic Cancer. *Cancer Cell* 2020;37:289–307.

67 Kim K-H, Kim S-J, Eccles JD, *et al*. Tumor immunogenicity regulates host immune responses, and conventional dendritic cell type 2 uptakes the majority of tumor antigens in an orthotopic lung cancer model. *Cancer Immunol Immunother* 2024;73:237.

68 Ansari AM, Ahmed AK, Matsangos AE, *et al*. Cellular GFP Toxicity and Immunogenicity: Potential Confounders in in Vivo Cell Tracking Experiments. *Stem Cell Rev Rep* 2016;12:553–9.

69 Gulhati P, Schalck A, Jiang S, *et al*. Targeting T cell checkpoints 41BB and LAG3 and myeloid cell CXCR1/CXCR2 results in antitumor immunity and durable response in pancreatic cancer. *Nat Cancer* 2023;4:62–80.

70 Lewis HL, Chakedis JM, Talbert E, *et al*. Perioperative cytokine levels portend early death after pancreatectomy for ductal adenocarcinoma. *J Surg Oncol* 2018;117:1260–6.

71 Wang T, Notta F, Navab R, *et al*. Senescent Carcinoma-Associated Fibroblasts Upregulate IL8 to Enhance Prometastatic Phenotypes. *Mol Cancer Res* 2017;15:3–14.

72 Zhong Z, Yang K, Li Y, *et al*. Tumor-associated macrophages drive glycolysis through the IL-8/STAT3/GLUT3 signaling pathway in pancreatic cancer progression. *Cancer Lett* 2024;588:216784.

73 Teijeira A, Garasa S, Ochoa MC, *et al*. IL8, Neutrophils, and NETs in a Collusion against Cancer Immunity and Immunotherapy. *Clin Cancer Res* 2021;27:2383–93.

74 Chen S-J, Lian G, Li J-J, *et al*. Tumor-driven like macrophages induced by conditioned media from pancreatic ductal adenocarcinoma promote tumor metastasis via secreting IL-8. *Cancer Med* 2018;7:5679–90.

75 Gong R, Chen X, Sun X, *et al*. Identification of FOXP3+ epithelial cells contributing to pancreatic proliferation and angiogenesis. *Am J Physiol Cell Physiol* 2024;326:C294–303.

76 Huang C, Li H, Xu Y, *et al*. BICC1 drives pancreatic cancer progression by inducing VEGF-independent angiogenesis. *Signal Transduct Target Ther* 2023;8:271.

77 Saito Y, Xiao Y, Yao J, *et al*. Targeting a chemo-induced adaptive signaling circuit confers therapeutic vulnerabilities in pancreatic cancer. *Cell Discov* 2024;10:109.

78 Chan Y-T, Tan H-Y, Lu Y, *et al*. Pancreatic melatonin enhances anti-tumor immunity in pancreatic adenocarcinoma through regulating tumor-associated neutrophils infiltration and NETosis. *Acta Pharm Sin B* 2023;13:1554–67.

79 Chaib S, López-Domínguez JA, Lalinde-Gutiérrez M, *et al*. The efficacy of chemotherapy is limited by intratumoral senescent cells expressing PD-L2. *Nat Cancer* 2024;5:448–62.

80 Yang C, Geng H, Yang X, *et al*. Targeting the immune privilege of tumor-initiating cells to enhance cancer immunotherapy. *Cancer Cell* 2024;42:2064–81.

81 Datta J, Dai X, Bianchi A, *et al*. Combined MEK and STAT3 Inhibition Uncovers Stromal Plasticity by Enriching for Cancer-Associated Fibroblasts With Mesenchymal Stem Cell-Like Features to Overcome Immunotherapy Resistance in Pancreatic Cancer. *Gastroenterology* 2022;163:1593–612.

82 Hosein AN, Dangol G, Okumura T, *et al*. Loss of Rnf43 Accelerates Kras-Mediated Neoplasia and Remodels the Tumor Immune Microenvironment in Pancreatic Adenocarcinoma. *Gastroenterology* 2022;162:1303–18.

83 Lesina M, Wörmann SM, Morton J, *et al*. RelA regulates CXCL1/CXCR2-dependent oncogene-induced senescence in murine Kras-driven pancreatic carcinogenesis. *J Clin Invest* 2016;126:2919–32.

84 Wang B, Hendricks DT, Wamunyokoli F, *et al*. A growth-related oncogene/CXC chemokine receptor 2 autocrine loop contributes to cellular proliferation in esophageal cancer. *Cancer Res* 2006;66:3071–7.

85 Purohit A, Saxena S, Varney M, *et al*. Host Cxcr2-Dependent Regulation of Pancreatic Cancer Growth, Angiogenesis, and Metastasis. *Am J Pathol* 2021;191:759–71.

86 von Hundelshausen P, Agten SM, Eckardt V, *et al*. Chemokine interactome mapping enables tailored intervention in acute and chronic inflammation. *Sci Transl Med* 2017;9:eaah6650.

87 Bell EW, Schwartz JH, Freddolino PL, *et al*. PEPPI: Whole-proteome Protein-protein Interaction Prediction through Structure and Sequence Similarity, Functional Association, and Machine Learning. *J Mol Biol* 2022;434:167530.

88 Sepuru KM, Poluri KM, Rajarathnam K. Solution structure of CXCL5--a novel chemokine and adipokine implicated in inflammation and obesity. *PLoS One* 2014;9:e93228.

89 Ravindran A, Sawant KV, Sarmiento J, *et al*. Chemokine CXCL1 dimer is a potent agonist for the CXCR2 receptor. *J Biol Chem* 2013;288:12244–52.

90 Kokkinos J, Ignacio RMC, Sharbeen G, *et al*. Targeting the undruggable in pancreatic cancer using nano-based gene silencing drugs. *Biomaterials* 2020;240.

91 Golan T, Khvalevsky EZ, Hubert A, *et al*. RNAi therapy targeting KRAS in combination with chemotherapy for locally advanced pancreatic cancer patients. *Oncotarget* 2015;6:24560–70.

92 Tsai WC, Strieter RM, Mehrad B, *et al*. CXC chemokine receptor CXCR2 is essential for protective innate host response in murine Pseudomonas aeruginosa pneumonia. *Infect Immun* 2000;68:4289–96.

93 Pugliese G, Liccardi A, Graziadio C, *et al*. Obesity and infectious diseases: pathophysiology and epidemiology of a double pandemic condition. *Int J Obes (Lond)* 2022;46:449–65.

94 Helms EJ, Berry MW, Chaw RC, *et al*. Mesenchymal Lineage Heterogeneity Underlies Nonredundant Functions of Pancreatic Cancer-Associated Fibroblasts. *Cancer Discov* 2022;12:484–501.